ORIGINAL RESEARCH

Self-Assembled Nanoparticles from Xie-Bai-San Decoction: Isolation, Characterization and Enhancing Oral Bioavailability

Wenlong Nie*, Yun Liu*, Jinshuai Lan, Ting Li, Yitian He, Zhe Li, Tong Zhang (ID), Yue Ding

School of Pharmacy, Shanghai University of Traditional Chinese Medicine, Shanghai, 201210, People's Republic of China

*These authors contributed equally to this work

Correspondence: Tong Zhang; Yue Ding, Email zhangtongshutcm@hotmail.com; Dingyue-2001@hotmail.com

Background: Natural nanoparticles have been found to exist in traditional Chinese medicine (TCM) decoctions. However, whether natural nanoparticles can influence the oral bioavailability of active compounds has not been elucidated. Using Xie-Bai-San decoction (XBSD) as an example, the purpose of this study was to isolate, characterize and elucidate the mechanism of the nanoparticles (N-XBSD) in XBSD, and further to explore whether the bioavailability of the main active compounds could be enhanced by N-XBSD.
Methods: N-XBSD were isolated from XBSD, and investigated its characterization and study of its formation mechanism, and evaluation of its ability to enhance bioavailability of active compounds.
Results: The N-XBSD was successfully isolated with the average particle size of 104.53 nm, PDI of 0.27 and zeta potential of −5.14 mV. Meanwhile, all the eight active compounds were most presented in N-XBSD. Kukoamine B could self-assemble with mulberroside A or liquiritin to form nanoparticles, respectively. And the FT-IR and HRMS results indicated the possible binding of the ammonium group of kukoamine B with the phenolic hydroxyl group of mulberroside A or liquiritin, respectively. The established UPLC-MS/MS method was accurate and reliable and met the quantitative requirements. The pharmacokinetic behaviors of the N-XBSD and decoction were similar in rats. Most notably, compared to that of free drugs, the C_{max}, $AUC_{0-\infty}$, AUC_{0-t}, $T_{1/2}$ and $MRT_{0-\infty}$ values of index compounds were the higher in N-XBSD, with a slower plasma clearance rate in rats.
Conclusion: The major active compounds of XBSD were mainly distributed in N-XBSD, and N-XBSD was formed through self-assembly among active compounds. N-XBSD could obviously promote the bioavailability of active compounds, indicating natural nanoparticles of decoctions play an important role in therapeutic effects.
**Keywords:** nanoparticles, enhancing bioavailability, comparative pharmacokinetics, UPLC-MS/MS, Xie-Bai-San decoction

Introduction

Traditional Chinese medicine (TCM) plays a crucial role in the prevention and treatment of various diseases, and is also known for its complexity of active compounds leading to multiple pharmacological activities.[1–3] Therefore, isolation and evaluation of phytochemicals from herbal to explain the mechanism of TCM has long been widely conducted. Frustratingly, many compounds purified from herbals are difficult to be absorbed, which severely limits their clinical applications.[4] According to relative study, the purified form of compounds showed significantly lower exposure level in the bloodstream after oral administration, compared with the herbal extracts taken in the form of traditional decoction.[5] For example, after oral administration of pure gentiopicroside the concentration level of gentiopicroside in the blood was lower than that of the group treated with of *Gentianae* decoctions.[6] Therefore, interactions between co-existing compounds in the decoction may affect the oral absorption and pharmacokinetic profile of these bioactive compounds.

Natural nanoparticles are widely present in TCM decoctions and have significant biological activity.[7–10] During decocting, phytochemicals in herbs or plant materials are dissolved in boiling water, forming a complex system with multiple phase states, including molecules, nanoaggregates, precipitates, and emulsions. It has been shown that the colloid-like aggregates

Graphical Abstract
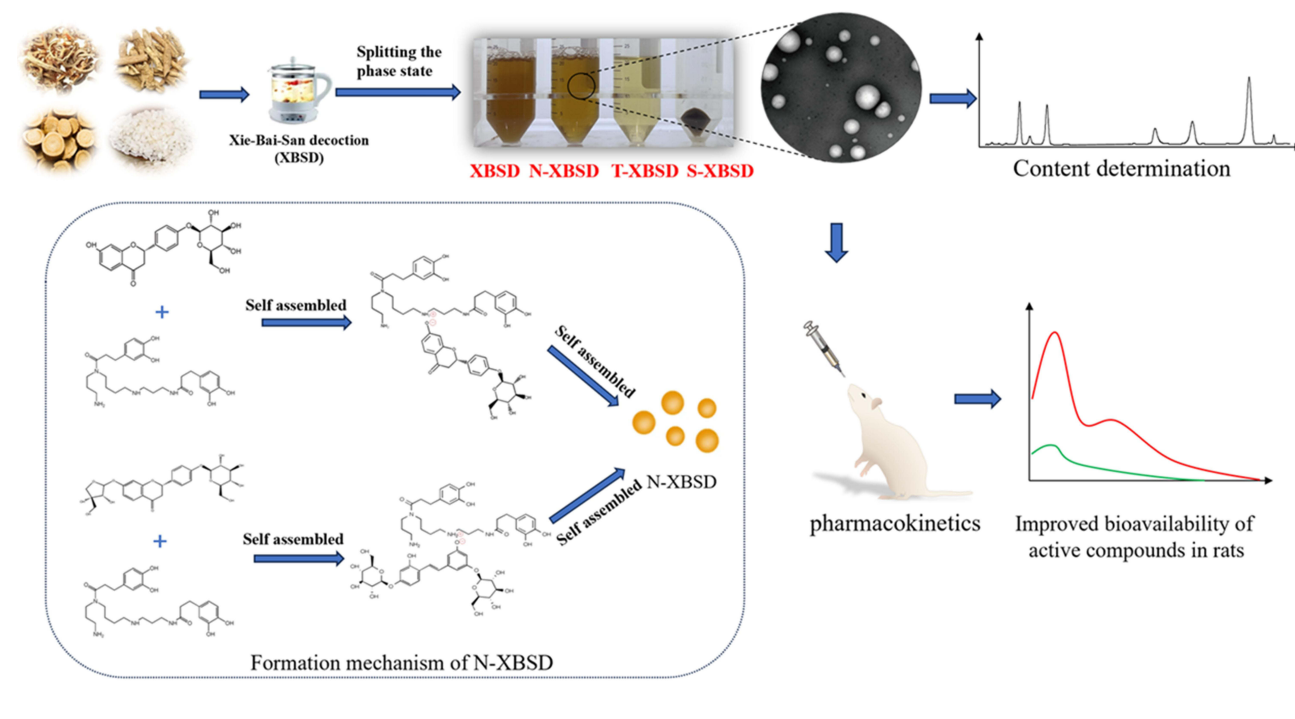
which formed naturally could be found in 60 herbs and 24 Chinese herbal formulas.[7] Researchers have partly explored formation mechanism, solubilization and pharmacological effects of nanoparticles. For example, Yang et al found that the mechanism of nanoparticles formation in Bai-Hu-Tang decoction was related to the formulation of the prescription.[8,9] The nanoaggregates in Ge-Gen-Qin-Lian-Tang decoction could increase the uptake of baicalin in Caco-2 cells and had a good antidiabetic activity on STZ-induced diabetic rats.[10] All these results illustrated that what an important role of nanoparticles have played in decoction and their significant effects on biological activity of decoction in clinic.

Xie-Bai-San decoction (XBSD) was first recorded in "Xiao'er Yao Zheng Zhi Jue" compiled by Yi Qian of the Song Dynasty and has been used for centuries in the clinical treatment of pediatric pneumonia in Asian countries.[11] XBSD is composed of four TCMs including Cortex Mori (the dried root bark of the *Morus alba* L), Cortex Lycii (the dried root bark of *Lycium chinense* Mill or *Lycium barbarum* L), Radix Glycyrrhizae (the dried roots and rhizomes of *Glycyrrhiza uralensis* Fisch, *Glycyrrhiza glabra* L, and *Glycyrrhiza inflata* Batalin) and Japonica rice. Cortex Mori is widely applied to treat pneumonia, with mulberroside A (Figure 1A) and mulberroside C (Figure 1B) as its main active compounds.[12–14] Cortex Lycii demonstrates pharmacological effects such as heat-resolving, analgesic, lipid-lowering and immune regulation,[15–17] and its main compound kukoamine B (Figure 1D) can inhibit the inflammatory response in septic mice.[18] Liquiritin (Figure 1F) and glycyrrhizic acid ammonium salt (Figure 1H) are the main compounds of Radix Glycyrrhizae, showing anti-inflammatory effect.[19–21] The liquiritin apioside (Figure 1G) in Radix Glycyrrhizae has antitussive and expectorant activities.[22] It can be deduced from the above materials that the active compounds of XBSD influence its efficacy. On the other hand, it is worth noting that glycyrrhizic acid is reported as a surfactant that can self-assembles into micelles in aqueous solution.[23] Besides, the Japonica rice contains a large number of polysaccharides and proteins, forming hydrophilic or hydrophobic colloids to increase the stability of solution after boiling in water.[8] The above results suggest that Japonica rice and Radix Glycyrrhizae in XBSD might contribute to forming nanoparticles. Proteins and polysaccharides may directly modify the existing forms as well as the intestinal absorption of active compounds.[24] Nanoparticles can adsorb active constituents and carry them for absorption.[24,25] These results suggest that nanoparticles in XBSD may also affect the effect by changing oral bioavailability of the active compounds. However, few systematic studies have been conducted to date.
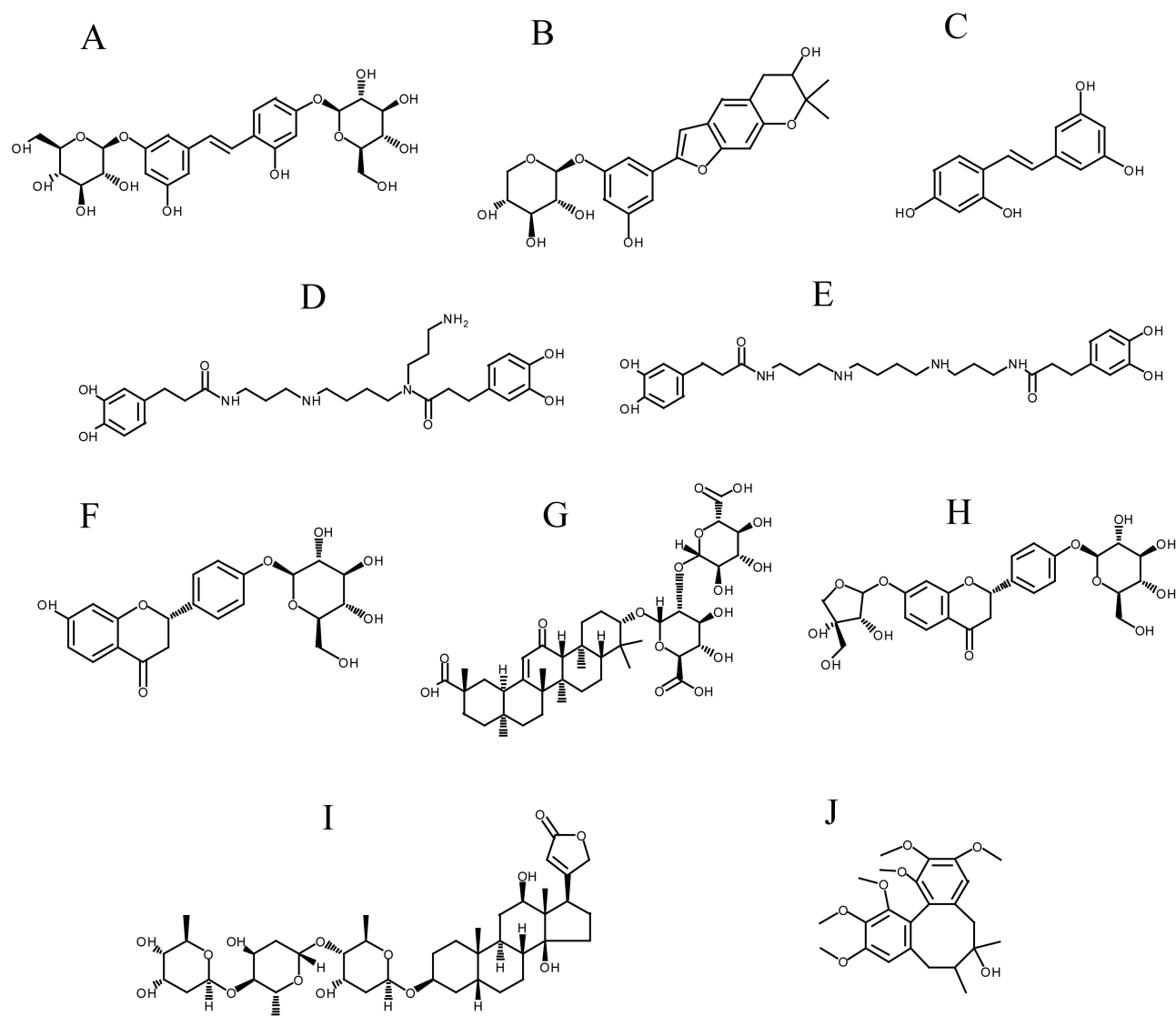
Figure 1 Chemical structures of mulberroside A (**A**), mulberroside C (**B**), oxyresveratrol (**C**), kukoaMine B (**D**), kukoaMine A (**E**), liquiritin (**F**), glycyrrhizic acid ammonium salt (**G**), liquiritin apioside (**H**), digoxin (**I**) (internal standard), schisandrin (**J**) (internal standard).

Accordingly, the objective of this study was to explore the property of N-XBSD to enhance the oral bioavailability of main active compounds in decoction. First, N-XBSD was isolated by high-speed centrifugation and characterized by particle size, zeta potential, transmission electron microscopy (TEM), and its gastrointestinal stability was investigated. To evaluate the ingredients of N-XBSD, a HPLC method for the simultaneous determination of eight active compounds of XBSD was developed. The formation mechanism of N-XBSD was investigated using Fourier transform infrared spectroscopy (FT-IR) and high-resolution mass spectrometry (HRMS). Moreover, to compare the pharmacokinetic profiles of XBSD, N-XBSD and free drugs, a UPLC-MS/MS method to rapidly and accurately determine the blood drug concentration of five major compounds was established and validated. In view of the widespread existence of nanoparticles in TCM decoctions, this study is expected to promote more research on natural nanoparticles playing an important role in therapeutic effects.

Materials and Methods
Materials
Cortex Mori (Batch number: PZ2021073001, Shanghai, China), Cortex Lycii (Batch number: YP2021080501, Shanghai, China) and Radix Glycyrrhizae (Batch number: PZ2021081901, Shanghai, China) were from Shanghai Kangqiao

traditional Chinese medicine Co. Ltd. Japonica rice (Batch number: PZ2021081901, Shandong, China) was purchased from Shandong Shangyao traditional Chinese medicine Co. Ltd. The standards which included mulberroside A, kukoamine A (Figure 1E), kukoaMine B, liquiritin, liquiritin apioside, glycyrrhizic acid ammonium salt, mulberroside C, oxyresveratrol (Figure 1C) and schisandrin (Figure 1J) (≥98% purity) were all purchased from Shanghai Yuanye Biotechnology Co., Ltd. (Shanghai, China). Digoxin (Figure 1I) was purchased from Merck KGaA (Darmstadt, Germany). 3500Da dialysis bag was purchased from Shanghai Yuanye Biotechnology Co., Ltd. (Shanghai, China).

Animals

We obtained male Sprague-Dawley rats (200–220 g) from Shanghai Sippr-BK Laboratory Animal Co., Ltd. (Shanghai, China). An ambient temperature of 22–24 °C and 60–65% relative humidity were used to raise rats in the Laboratory Animal Center of Shanghai University of Traditional Chinese Medicine. Rats were fed and watered normally.

Preparation of Standard XBSD

According to the "Xiao'er Yao Zheng Zhi Jue", a famous formulary in TCM, compiled by Yi Qian. The preparation of XBSD was performed as follows: Cortex Mori (39.3 g), Cortex Lycii (39.3 g), Radix Glycyrrhizae (3.93 g) and Japonica rice (10 g) were crushed into coarse powder and then soaked in 1200 mL of distilled water for 15 minutes. Then boil with high heat and simmer to 840 mL. Lastly, filter with four layers of gauze to get XBSD.[26]

Separation of the Phase States in XBSD

The 50 mL XBSD (I) was centrifuged for 30 min (4000 rpm). The supernatant was tightly sealed in a dialysis bag, and then submerged into 500 mL water and dialyzed at 37°C for 1 h (120 rpm). Finally, the liquid in the dialysis bag was centrifuged for 30 min (13,000 rpm). The dialysis and centrifugation were repeated twice. By the above operation, all the centrifuged precipitates were collected, ie, the sediment phase state (S-XBSD, II), the dialysis outer liquid was the true solution phase state (T-XBSD, III), and the liquid inside the dialysis bag was the nanoparticles (N-XBSD, IV) (Figure 2).

TEM and Particle Size Analyser

One drop of XBSD and N-XBSD, was spread uniformly on a copper mesh coated with carbon film, respectively, dried, stained with 2.0% phosphotungstic acid for 2 min, dried again and the morphology of the nanoparticles was observed under transmission electron microscopy (TEM, Tokyo, Japan). A Zetasizer Nano ZSE (Malvern Zetasizer Nano-ZS ZEN 3600, Marvin, England) was used to determine the particle size distribution and surface potential of N-XBSD.
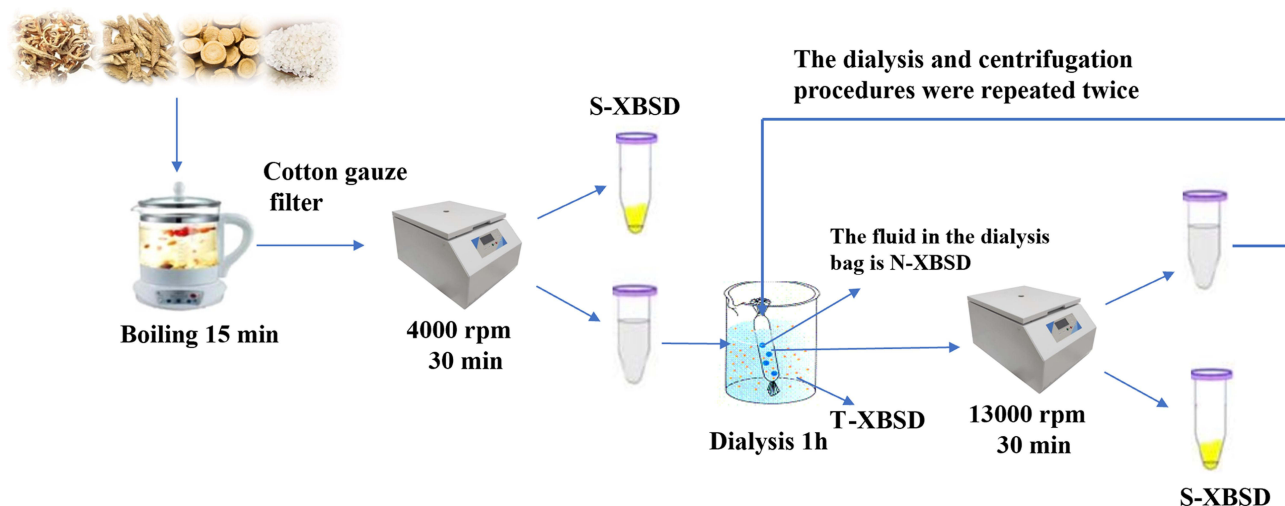

Figure 2 Isolation method of N-XBSD.

The Storage Stability and Gastrointestinal Stability

The storage stability of N-XBSD was examined at each time point. The N-XBSD were incubated in simulated gastric fluid (SGF, pH = 1.2), simulated intestinal fluid (SIF, pH = 6.8), and simulated colonic fluid (SCF, pH = 7.4) for 12 h, respectively. The particle size of the N-XBSD at 2, 4, 8 and 12 h were detected to access the storage stability and gastrointestinal stability of N-XBSD.

Chromatographic Conditions of HPLC-DAD Analysis

Analysis was performed using an HPLC system (Agilent Technologies, Santa Clara, CA, USA). The samples were separated by Agilent SB-AQ column (150 mm × 3.5 mm, 2.7μm). The mobile phase was 0.1% (v/v) trifluoroacetic acid (solvent system A) and acetonitrile (solvent system B). The gradient elution method after optimization was performed as follows: 0–5 min, 98% A; 5–15 min, 98%–90%A; 15–38 min, 90%–82%A; 38–45 min, 82%A, 45–55 min, 82%–70%A; 55–60 min, 70%–50%A; 60–65 min, 50%–25%A; 65–70 min, 5%A. The flow rate was set at 0.3 mL/min and the injection volume was 2 μL. The column temperature was set at 25°C. The detection wavelengths of the DAD detector were performed as follows: 324 nm for 0–22 min, 282 nm for 22–30 min, 276 nm for 30–43 min, 330 nm for 43–55 min and 254 nm for 55–70 min.

Primary stock solutions of mulberroside A (426.15 μg/mL), kukoaMine B (811.50 μg/mL), kukoamine A (75.05 μg/mL), liquiritin (50.74 μg/mL), liquiritin apioside (55.37 μg/mL), oxyresveratrol (48.02 μg/mL), glycyrrhizic acid ammonium salt (109.80 μg/mL), and mulberroside C (65.15 μg/mL) were prepared in 50% methanol. After gradient dilution, calibration curves were obtained for five concentration levels. By comparing retention times (RT) and UV spectra with those of standard compounds (mulberroside A, kukoaMine B, kukoamine A, liquiritin, liquiritin apioside, oxyresveratrol, glycyrrhizic acid ammonium salt and mulberroside C), chromatographic peaks were identified. 5 mL of XBSD, N-XBSD and T-XBSD were respectively placed in 10 mL volumetric bottles, 5 mL methanol was added to the scale, swirled for 10 min, and then filtered by 0.22 μm organic filter membrane for HPLC analysis. The S-XBSD was taken from 50 mL of the decoction and added into 10 mL of 50% methanol solution, then ultrasounded for 20 min and filtered by 0.22 μm organic filter membrane for HPLC analysis.

Study of the Mechanism of N-XBSD Formation
Self-Assembly Formation

KukoaMine B was combined with mulberroside A and liquiritin in the ratio of 1:1 (0.2 mM) at 120 °C, respectively. The solution was heated and stirred without reflux condensation until the concentration increased to 4 mM. A deepening of the color of the solution was observed, and the Tyndall effect was obvious.

Characterization of Self-Assemblies

The size, particle size distribution and surface potential of the self-assembled nanoparticles were determined using a Zetasizer Nano ZSE (Malvern Zetasizer Nano-ZS ZEN 3600, Marvin, England). The infrared spectra of monomers, physical mixtures and nanoparticles in the range of 4000–400 cm^{-1} were determined by FTIR spectroscopy (Thermo, Florida, USA). HRMS (Agilent 6545 LC/Q-TOF, Agilent Technologies, Santa Clara, CA, USA) was used to analyze the basic units of two self-assembled nanoparticles.

Pharmacokinetic Study
Mass Spectrometry System for Qualitative Analysis

An Agilent 6460 series MS/MS system (Agilent Technologies, Santa Clara, CA, USA) was combined with an Agilent 1290 UPLC system (Agilent Technologies, Santa Clara, CA, USA) to quantify analytes in ESI+ and ESI- ionization modes. The capillary voltage was set to 4000 V and gas flow rate was 10 L/min. The nebulization gas pressure was 30 psi and the gas temperature was 350°C. A gradient elution of 0.1% (v/v) formic acid (solvent system A) and acetonitrile (solvent system B) at 0.4 mL/min was used to achieve the ideal results on Agilent EC-C18 column (2.1 mm × 100 mm, 1.8 μm) with the following process. The gradient elution method for mulberroside A, liquiritin, liquiritin apioside and glycyrrhizic acid ammonium salt was 90% A in 0–1 min, 90–64% A in 1–3 min, 64–52% A in 3–4 min, 52–10% A in 4–

5 min, 10% A in 5–6 min, 10–90% A in 6–6.1 min, 90% A in 6.1–8 min. The gradient elution method for kukoaMine B was 95–92% A in 0–7 min, 92–5% A in 7–8 min, and 95% A in 8.1–10 min. The injection volume was 5 µL. The mass spectrometric parameters under multiple reaction monitoring (MRM) are shown in Table S1.

Sample Preparation

The IS (schisandrin) solution (50 ng/mL) and the IS (digitonin) solution (500 ng/mL) were mixed for five minutes in a 1.5 mL centrifuge tube containing 50 µL rat plasma. Then added 500 µL methanol, vortex for 20 minutes, and centrifuge for 10 min at 4°C (13,000 rpm). Transferred the entire supernatant to another 1.5 mL centrifuge tube and gently dried at 37°C under a nitrogen stream. Then, add 50 µL of 10% methanol to reconstitute. 5 µL of the supernatant was extracted and injected onto a column for analysis after centrifugation at 4°C for 10 minutes (13,000 rpm).

Method Validation

The validation parameters of the method include specificity, linearity, precision and accuracy, matrix effects, recovery, and stability.

Specificity

By comparing MRM chromatograms of rat blank plasma, blank plasma containing five analyzed compounds, and IS, plasma samples of rats after oral administration of XBSD for 2 h, specificity was assessed.

Linearity

Blank plasma samples were determined with 8 concentration levels of analytes. The standard curve was obtained by linear regression analysis with the ratio of peak area of the substance to be measured to the peak area of the internal standard (IS) Y as the vertical coordinate and the mass concentration of each substance X as the horizontal coordinate. The limit of quantification (LOQ) was also calculated according to the signal-to-noise ratio (S/N≥10).

Precision and Accuracy

Six replicates of three different concentrations (low, medium, and high) of quality control (QC) samples on the same day and three consecutive days were used to determine precision and accuracy, respectively. The relative error (RE, %) and relative standard deviation (RSD, %) were calculated according to theoretical concentrations and experimental results.

Extraction Recovery and Matrix Effect

The extraction recovery rate was measured by comparing the ratio of peak area to internal standard in the blank plasma sample with analyte added before extraction and the sample with analyte added after extraction at three different concentrations (low, medium and high). Matrix effect was measured at three QC levels by comparing the peak areas of the extracted blank plasma samples with analyte and the corresponding pure standard solution.

Stability

The stability of the five analytes in rat plasma was determined by performing six replicates of QC samples at low, medium and high concentrations under different conditions. Short-term stability included the stability of plasma samples placed in the injector at 4°C for 24 h, and the stability of plasma samples after three freeze-thaw cycles at −20°C. Long-term stability was examined for the stability of plasma samples placed in the refrigerator at −80°C for 30 days.

Application to Pharmacokinetic Analysis

The SD rats were randomly assigned to 3 groups: XBSD, N-XBSD and free drugs group, with 6 rats in each group. The XBSD and N-XBSD groups were administered orally at a dose of 12.5 g of raw herb/kg. The levels of the five compounds of N-XBSD, mulberroside A, kukoaMine B, liquiritin, liquiritin apioside and glycyrrhizic acid ammonium salt, were determined by HPLC. The free drugs group was administered at same dose as the N-XBSD group. At 0.083, 0.17, 0.25, 0.5, 0.75, 1, 2, 4, 6, 8, 12, 24 h after oral administration, blood samples (0.2 mL) were collected into the

heparinized centrifuge tube via the ophthalmic venous plexus. After centrifugation at 4°C (4000 rpm) for 10 min, the supernatant was transferred to a 1.5 mL centrifuge tube and stored at −80°C until the samples were analyzed.

Statistical Analysis

Important pharmacokinetic parameters, including C_{max} (the maximum plasma concentration), $T_{1/2}$ (the terminal elimination half-life), T_{max} (time to reach C_{max}), AUC_{0-t} (the area under curve from time zero to time t), $AUC_{0-\infty}$ (the area under curve from time zero to time infinity), CLz/F (clearance corrected for bioavailability) and MRT_{0-t} (mean residence time from time zero to time t) were calculated using DAS 2.0 software. Statistical calculations were performed using SPSS 21.0 software.

Results

Separation of Nanoparticles from XBSD

N-XBSD was separated by high-speed centrifugation combined with dialysis, which is a common method for separating nanoparticles from decoctions.[8,27] Briefly, the dialysis was utilized to remove free drugs from the decoction and then high-speed centrifugation was used to remove the micron-sized particles to finally obtain N-XBSD, which showed an obvious Tyndall phenomenon (Figure 3C). The TEM results showed that nanoparticles were present in XBSD but contained more micrometer-sized particles (Figure 3A), whereas N-XBSD was spherical with diameters ranging from 30 to 500 nm (Figure 3B). The average particle size, polydispersity index (PDI) and zeta potential of N-XBSD were 104.53 ± 2.63 nm, 0.27 ± 0.01 (Figure 3C) and −5.14±0.55 mV, respectively (Figure 3D), which indicated a homogeneous particle. In the stability study, the particle size of N-XBSD did not change significantly not only in storage but also in SGF (pH=1.2), SIF (pH=6.8), and SCF (pH = 7.4) for 12 h (Figure 3E and F). This showed that N-XBSD could tolerate strong acid and protease decomposition after oral administration.

Determination of the Chemical Composition of XBSD, S-XBSD, T-XBSD and N-XBSD by HPLC

In order to study the distribution of active compounds, the chemical composition of XBSD, S-XBSD, T-XBSD and N-XBSD were analyzed by HPLC, including mulberroside A, kukoaMine B, kukoamine A, liquiritin, liquiritin apioside, oxyresveratrol, glycyrrhizic acid ammonium salt and mulberroside C. The chromatogram is shown in Figure 4. And the linearity, sensitivity, precision, accuracy, recovery and stability of the eight analytes were summarized in Tables S2–S4. These results showed that the concentration of the analytes showed a good relationship with the peak area in the detection range (R ≥ 0.9998). The limits of detection (LOD) and limits of quantification (LOQ) were in the range of 0.17–0.97 μg/mL and 0.57–3.23 μg/mL, respectively. The overall RSDs for precision and repeatability were not more than 3.21% and 3.41%, respectively. The developed method had an acceptable accuracy with analytes recoveries of 95.84–102.60% for all analytes. In terms of stability, the RSD of the concentration of each analyte was less than 2.97% within 24 h. The above results showed that the established method has good linearity, sensitivity, precision, accuracy, recovery and stability, and can be used for the quantitative analysis of eight compounds in XBSD.

As shown in Table 1, the distribution of the above compounds showed significant differences in different phase states. The percentages of mulberroside A, kukoaMine B, kukoamine A, liquiritin, liquiritin apioside, oxyresveratrol, glycyrrhizic acid ammonium salt and mulberroside C in N-XBSD were 80.3%, 83.51%, 85.52%, 59.14%, 83.08%, 74.64%, 82.70% and 66.57%, respectively, of the total contents in XBSD. These results indicate that the active compounds in XBSD are mainly distributed in N-XBSD.

The Mechanism of N-XBSD Formation

Mulberroside, kukoaMine B and liquiritin are the main active constituents of Cortex Mori, Cortex Lycii and Radix Glycyrrhizae, respectively. It is noteworthy that the contents of mulberroside A, kukoaMine B and liquiritin were significantly higher in N-XBSD than in other phases. Therefore, we hypothesized that self-assembly may occur between them.

As shown in Figure 5A and B, kukoaMine B was heated and stirred with mulberroside A and liquiritin forming MUL-KUB NPs and LIQ-KUB NPs respectively, both of which were around 200 nm. FT-IR and HRMS were performed to
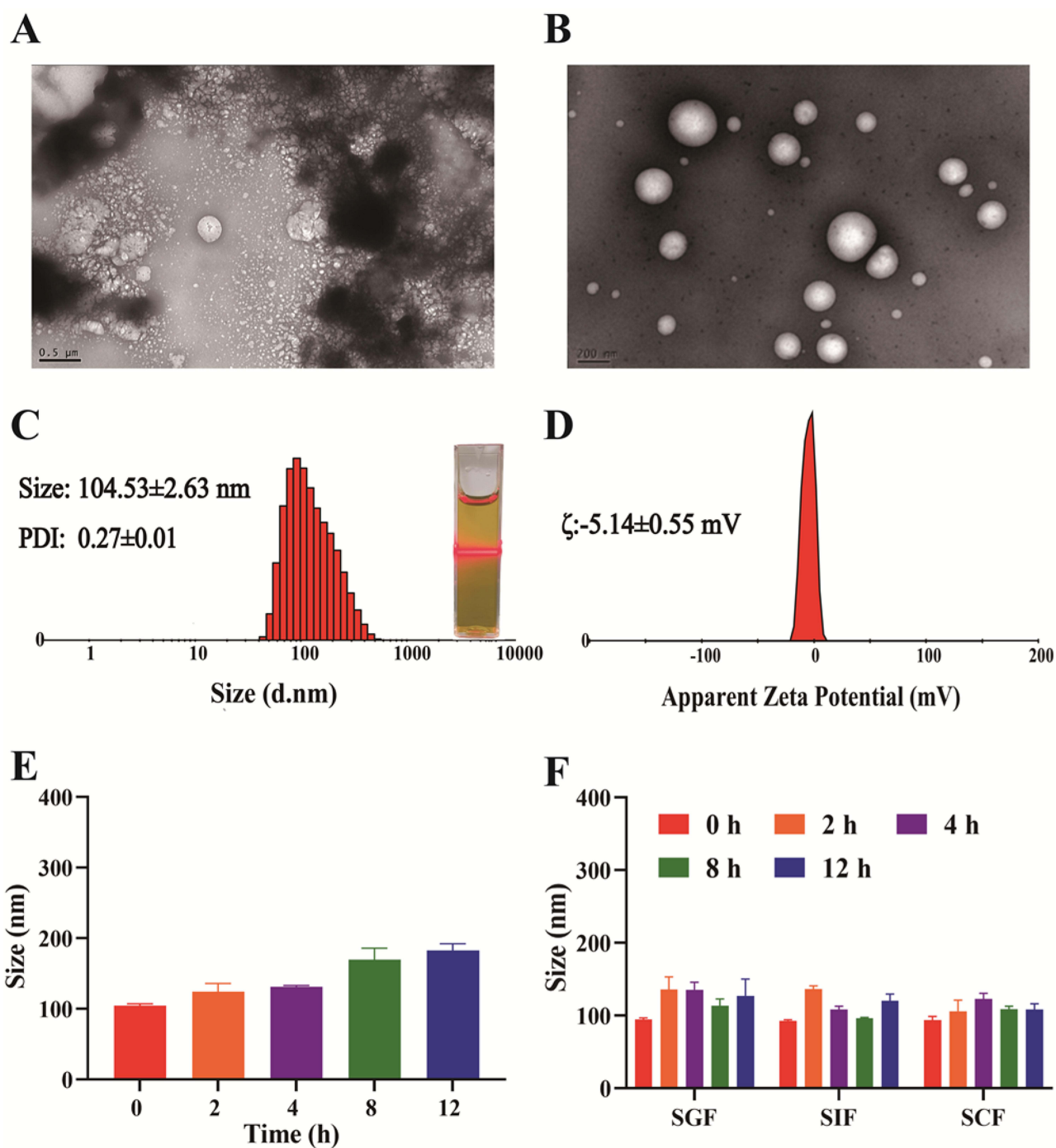
Figure 3 (**A**) TEM images of XBSD. (**B**) TEM images of N-XBSD. (**C**) Particle size distribution of N-XBSD. (**D**) The zeta potential of N-XBSD. (**E**) Size changes of N-XBSD in water. (**F**) Size changes of N-XBSD in SGF (pH=1.2), SIF (pH=6.8) and SGF (pH=7.4).

investigate the formation mechanism of nanoparticles. In the physical mixture of MUL-KUB, the peak at 3377.38 cm^{-1} (Figure 5C) was attributed to the stretching vibrations of the phenolic hydroxyl groups on the benzene rings of mulberroside A. However, in MUL-KUB NPs, the peak was shifted to 3411.94 cm^{-1}. Similarly, the peak at 1137.34 cm^{-1} was attributed to the stretching vibration of C-N in kukoaMine B, but the peak was shifted to a higher wavenumber (1185.01 cm^{-1}) in the MUL-KUB NPs. In HRMS, a deprotonated mulberroside A/kukoaMine B complex with a binding ratio of 1:1 (*m/z* 1099.4845) was observed in the ESI+ mode (Figure 5E), and its secondary fragments masses of *m/z* 531.3122 and m/z
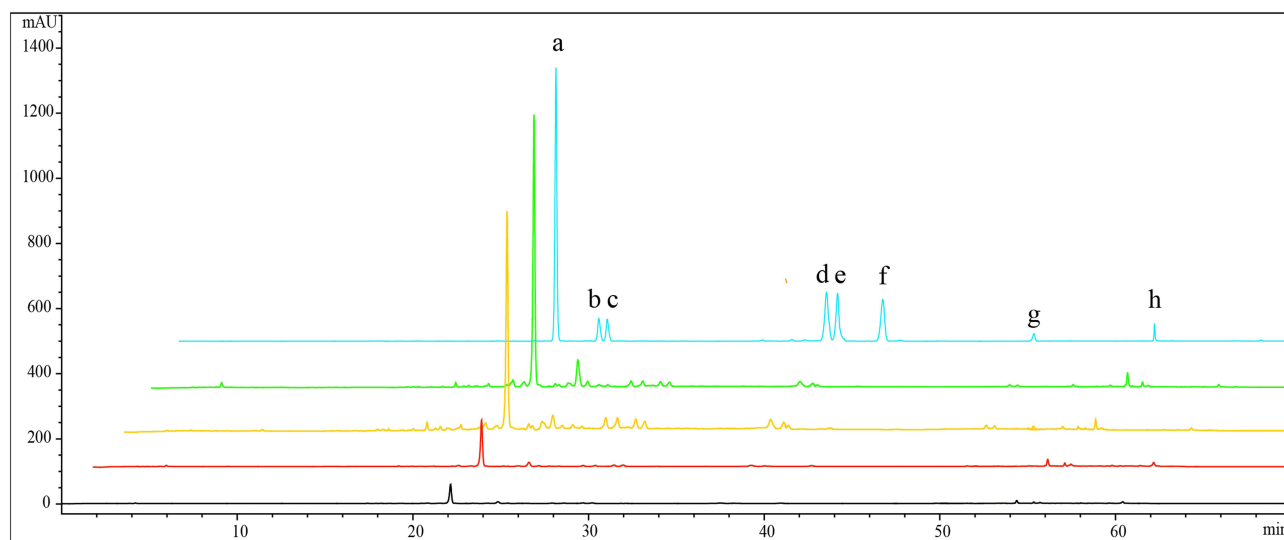
Figure 4 A representative HPLC chromatogram. From top to bottom: mixture of standard compounds (blue line), XBSD (green line), N-XBSD (Orange line), T-XBSD (red line) and S-XBSD (black line). (a) mulberroside A; (b) kukoaMine B; (c) kukoaMine A; (d) liquiritin; (e) liquiritin apioside; (f) oxyresveratrol; (g) mulberroside C; (h) glycyrrhizic acid ammonium salt.

591.1656 corresponded to mulberroside A and kukoaMine B+Na, respectively. This may be due to the electrostatic interaction between the phenolic hydroxyl in mulberroside A and the ammonium ions in kukoaMine B. The results observed in the self-assembly of liquiritin and mulberroside A are also consistent. The peak at 3370.22 cm^{-1} (Figure 5D) was attributed to the stretching vibrations of the phenolic hydroxyl groups of liquiritin. However, in LIQ-KUB NPs, the peak was shifted to a lower wavenumber (3351.00 cm^{-1}). In HRMS, a deprotonated liquiritin/kukoaMine B complex with a binding ratio of 1:1 (*m/z* 947.3925) was observed in the ESI- mode (Figure 5F), and its secondary fragments masses of *m/z* 529.2989 and *m/z* 417.1155 correspond to liquiritin and kukoaMine B, respectively. This may be due to the electrostatic interaction between the phenolic hydroxyl in liquiritin and the ammonium ions in kukoaMine B. FT-IR and HRMS directly confirmed the self-assembly between the two groups of molecules.

Comparative Pharmacokinetics of XBSD, N-XBSD and Free Drugs After Oral Administration in Rats

In order to compare the pharmacokinetic differences between XBSD, N-XBSD and free drugs, a UPLC-MS/MS method was established for determining five representative drugs in rat plasma, namely mulberroside A, kukoaMine B, liquiritin, liquiritin apioside and glycyrrhizic acid ammonium salt.

Table 1 Determination of the Chemical Composition of XBSD, N-XBSD, S-XBSD and T-XBSD

| Compounds	XBSD (µg mL^{-1})	Percentage Content of N-XBSD(%)	Percentage Content of S-XBSD(%)	Percentage Content of T-XBSD(%)
Mulberroside A	300.76	80.83	2.89	16.28
KukoaMine B	154.73	83.51	2.01	14.48
Kukoamine A	36.71	85.52	2.25	12.23
Liquiritin	15.73	59.14	28.84	12.02
Liquiritin apioside	10.73	83.08	12.75	4.17
Oxyresveratrol	2.70	74.64	4.63	20.73
Glycyrrhizic acid ammonium salt	10.17	82.70	10.50	6.8
Mulberroside C	1.75	66.57	7.06	26.37
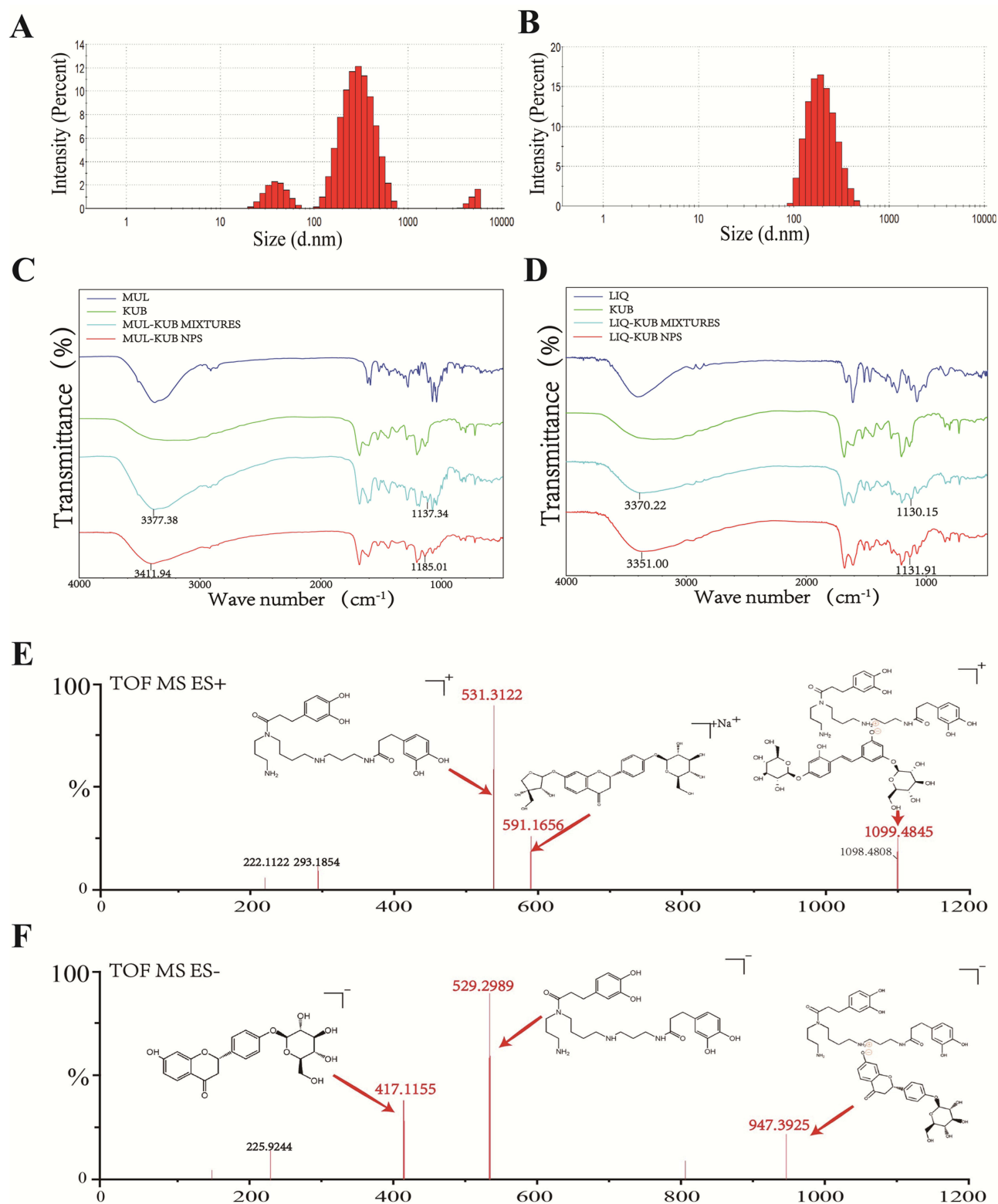
Figure 5 (**A**) Particle size of MUL-KUB NPs. (**B**) Particle size of LIQ-KUB NPs. (**C**) FT-IR of MUL-KUB NPs, their monomers and their mixtures. (**D**) FT-IR of LIQ-KUB NPs, their monomers and their mixtures. (**E**) ESI-HRMS spectrum of MUL-KUB NPs. (**F**) ESI-HRMS spectrum of LIQ-KUB NPs. (The FT-IR spectra obtained after OMNIC 9.9.473 software processing in sub (**C** and **D**). The red arrow point to the ion peaks corresponding to the structural formula of the compound and the red text represent the mass-to-charge ratio (*m/z*) of the ion peaks in sub (**E** and **F**).

Method Validation

Specificity

Figure 6 shows typical MRM chromatograms of blank plasma, plasma spiked with analyses and IS, and plasma samples from rats after 2 h of oral administration of drugs. There was no interference between the analyses and the IS during the retention time, and the peak shape was good, indicating the good specificity of the method.

Linearity and LLOQ

The regression equations, linear ranges and LLOQ of the standard curves for five compounds to be measured in rat plasma was shown in Table S5. The linear ranges of mulberroside A, kukoaMine B, liquiritin, liquiritin apioside and glycyrrhizic acid ammonium salt were 18.42–589.38, 13.13–1680.200, 3.94–1259.64, 1.68–672.31, 1.26–504.65, 1.681–672.31 and 1.26–504.65 ng/mL, respectively, and the correlation coefficients r of the standard curves were all greater than 0.995, indicating that the linearity was good and could be used for the determination of plasma sample content.

Precision and Accuracy

Table S6 shows the intra-day and inter-day precision results for the five analytes. The intra-day accuracy range (RSD) was 1.17–6.55%; intra-day accuracy range (RE) was −10.8–1.87%, inter-day accuracy range (RSD) was 1.60–12.85%; inter-day accuracy range (RE) was −13.67–13.28%, and all of them met the criteria. According to the results, the established method was reproducible, accurate, and could be used for the quantitative analysis of the five analytes.

Extraction Recovery and Matrix Effect

The average extraction recoveries and matrix effects for the five compounds at three QC levels were summarized in Table S7. The recoveries ranged from 28.59% to 102.53% for the three QC samples of the five analytes, and the matrix effects ranged from 89.40% to 114.31%. The results indicated that the recoveries and matrix effects of the established analytical methods were acceptable.

Stability

The results in Table S8 showed that five compounds in rat plasma remained stable and met the analytical criteria in plasma samples when stored at −80°C for 30 days, repeated freeze-thaw cycles three times, and stored at 4°C for 24 h.

Comparative Analysis of Pharmacokinetic Results in Rats

The pharmacokinetics were compared after oral administration of XBSD, N-XBSD and free drugs using UPLC-MS/MS. The mean concentration–time curves of the drugs in the plasma of the rats from the XBSD group, the N-XBSD group, and the free drugs group were shown in Figure 7. Pharmacokinetic parameters, including $T_{1/2}$, T_{max}, C_{max}, AUC_{0-t}, $AUC_{0-\infty}$, CLz/F and MRT_{0-t} were calculated using DAS 2.0 software as shown in Table 2.

The results showed that the five compounds exhibited similar pharmacokinetic profiles in N-XBSD and XBSD groups, which might be attributed that five compounds of XBSD present as nanoparticles. While there was a significant difference in the pharmacokinetic behavior between N-XBSD and free drugs. Compared to the free drugs, the mean $T_{1/2}$ of mulberroside A, kukoaMine B, ligiritin, liquiritin apioside and glycyrrhizic acid ammonium salt in the N-XBSD group were prolonged by 236.48, 69.54, 55.91, 132.20, and 96.17%, respectively. The C_{max} of kukoaMine B was significantly higher in the N-XBSD group ($p<0.05$). The mean AUC_{0-t} of mulberroside A, kukoaMine B, ligiritin, liquiritin apioside and glycyrrhizic acid ammonium salt in the N-XBSD group were increased by 122.73, 153.76, 112.30, 79.17, and 95.25%, respectively; and the mean AUC_{0-t} of kukoaMine B, ligiritin, liquiritin apioside, and glycyrrhizic acid ammonium salt were significantly higher in rats of the N-XBSD group than that of free drugs group rats ($p<0.05$). The CLz/F of mulberroside A and liquiritin apioside were significantly lower in the N-XBSD group than that of the free drugs group ($p< 0.05$). Compared with the free drug group, all five compounds in N-XBSD exhibited similar pharmacokinetic profiles to the extended-release formulation after oral administration to rats. Synthesized the above results, the apparent feature showed that N-XBSD significantly enhanced the oral bioavailability of active compounds.
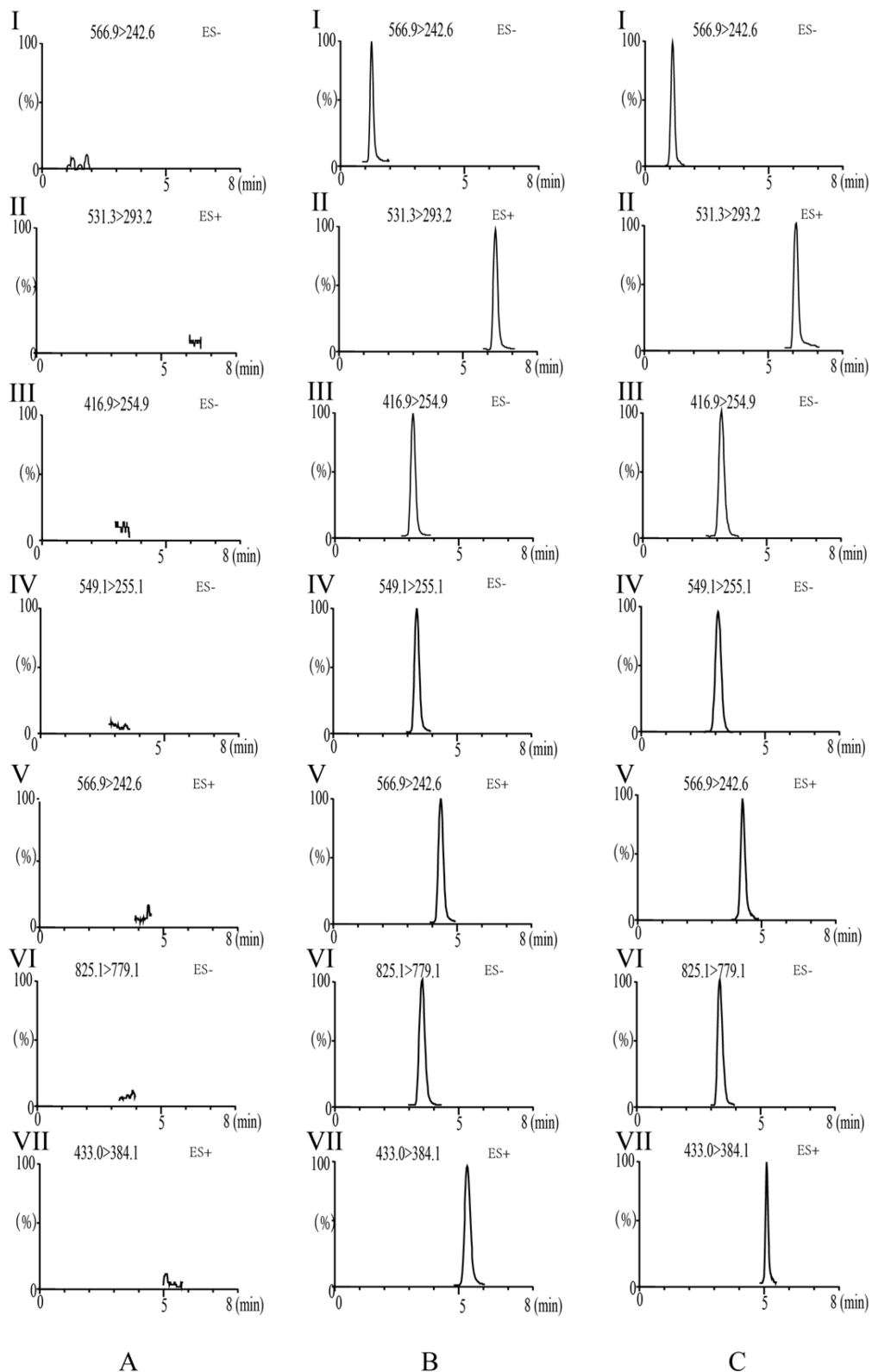
Figure 6 Representative MRM chromatograms of (I) mulberroside A, (II) kukoaMine B, (III) liquiritin, (IV) liquiritin apioside, (V) glycyrrhizic acid ammonium salt, (VI) digoxin (IS), (VII) schisandrin (IS) in rat plasmas: (**A**) MRM chromatograms of blank plasma samples, (**B**) blank spiked with combined standard solutions of the five analytes and IS, (**C**) rat plasma samples at 2 h after oral administration of XBSD.
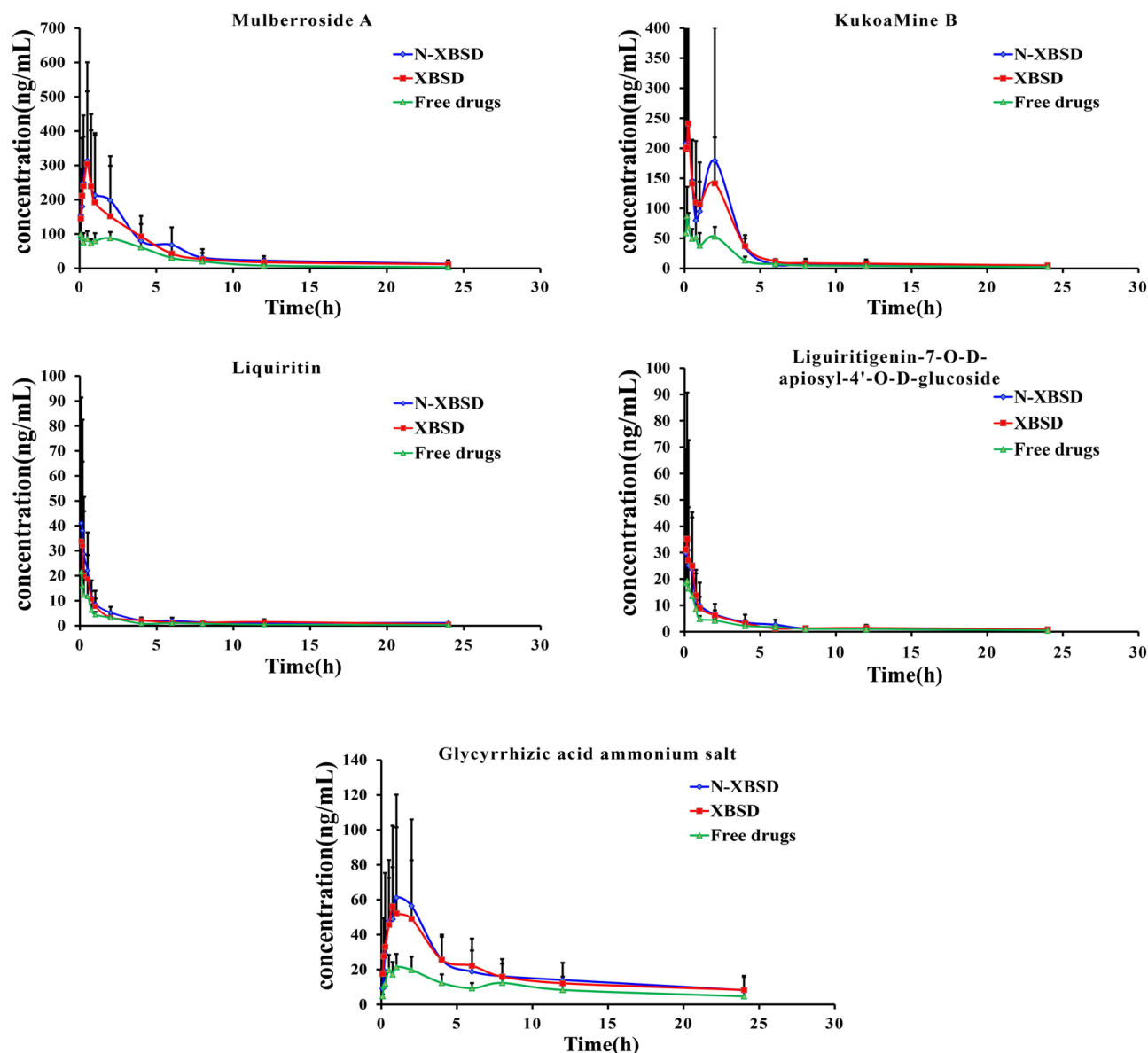
Figure 7 Mean plasma concentration–time curves of five major bioactive compounds after the oral administration of N-XBSD, XBSD and free drugs. The inserted figures show the initial 4 h profiles for the analytes.

Discussion

Nanoparticles can be separated by gel chromatography, centrifugation, ultrafiltration, etc.[11,27,28] Currently, the most commonly used method for separating nanoparticles in decoction is dialysis combined with centrifugation. It is generally accepted that dialysis bags are permeable to low-molecular-weight compounds. Therefore, the dialysis bag with a cutoff molecular weight of 3500 D was sufficient to permeate the free drug, but interestingly, it is unusual to detect mulberroside A, kukoaMine B, kukoamine A, liquiritin, liquiritin apioside, oxyresveratrol, glycyrrhizic acid ammonium salt and mulberroside C in the dialysis bag; all are small molecules with the molecular masses of 568.5, 530.7, 530.7, 418.4, 550.5, 244.2, 840.0 and 458.5, respectively. This suggests that these chemical compounds may be attached or embedded in the nanoparticles and involved in nanoparticles formation. Conventional nanocarriers are difficult to maintain stability in the gastrointestinal tract, eg, liposomes are unstable within acidic environments, leading to early release of active ingredients and low bioefficacy.[29] This does limit the use of liposomes in oral drug delivery. In the gastrointestinal stability experiment, we for the first time found that N-XBSD remained stable in gastrointestinal simulants for 12 h,

Table 2 Pharmacokinetic Parameters of Five Compounds in Male SD Rats After Oral Administration of N-XBSD, XBSD and Free Drugs (Mean ± SD, N = 6)

Compound	Groups	$T_{1/2}$(h)	T_{max}(h)	C_{max}(ng/mL)	AUC_{0-t} (ng/mL*h)	$AUC_{0-\infty}$ (ng/mL*h)	CLz/F (mL/h/kg)	$MRT_{0-\infty}$(h)
Mulberroside A	N-XBSD	7.59±4.06	0.33±0.16	334.55±180.78	1281.79±554.00*	1302.30±549.20*	12.13±10.71*	12.13±10.71
	XBSD	6.89±6.29	1.02±1.67	483.68±267.66*	961.64±371.53	1045.45±419.39	11.82±9.76	11.82±7.96
	Free drugs	3.84±1.96	0.50±0.84	120.20±19.12	575.50±95.07	589.86±107.66	20.57±3.26	5.12±1.42
KukoaMine B	N-XBSD	24.12±18.97	0.97±0.96	489.48±260.85*	648.31±357.73*	840.79±296.48*	20.37±12.53	21.45±20.76
	XBSD	14.47±23.26	0.65±0.76	299.82±315.25	631.73±237.55*	721.14±233.94*	16.09±3.83*	14.27±18.51
	Free drugs	10.22±3.18	0.55±0.81	95.15±44.16	255.48±62.85	288.21±67.22	31.38±9.22	9.41±2.65
Liquiritin	N-XBSD	12.30±10.40	0.16±0.08	44.02±48.33	61.24±20.19**	86.30±32.79**	61.23±27.72*	16.36±10.99
	XBSD	13.21±4.60	0.20±0.17	49.83±43.06	52.25±14.08*	61.85±12.18*	66.43±19.04*	13.00±3.89
	Free drugs	8.71±3.97	0.18±0.18	30.00±25.91	29.27±6.26	33.02±7.04	112.50±21.06	9.59±5.26
Liquiritin apioside	N-XBSD	12.43±7.69*	0.23±0.17	41.05±38.22	73.55±28.18*	89.80±21.77*	32.69±8.71*	14.859±10.48
	XBSD	10.47±6.18*	0.27±0.28	79.79±54.59	68.01±11.56*	82.35±25.85*	40.48±17.21*	11.07±8.05
	Free drugs	6.27±3.75	0.23±0.15	28.19±18.56	41.05±12.28	43.45±15.67	60.52±19.34	8.47±1.82
Glycyrrhizic acid ammonium salt	N-XBSD	14.58±8.08	0.55±0.27	71.17±54.72	452.61±221.15*	686.85±470.50*	8.96±7.20	19.09±12.82
	XBSD	11.23±8.93	1.23±1.59	76.78±43.30	428.28±162.35	568.22±153.49	6.97±2.12	13.72±4.83
	Free drugs	9.88±6.07	1.85±1.39	25.53±4.97	231.81±40.72	280.65±63.28	11.98±3.78	11.78±5.48

Notes: *ANOVA* test was used to calculate the significance of the differences, *$p < 0.05$ which compared with the free drugs; **$p < 0.01$ which compared with the free drugs.

suggesting that N-XBSD can tolerate decomposition by gastric acid and proteases. Hence, the nanoparticles in decoctions that can maintain their nanomorphology in the gastrointestinal tract are promising natural nano-carriers of oral drugs.

At present, the formation mechanism of nanoparticles in decoction is rarely reported, and the molecular formation mechanism of such pharmacologically valuable natural nanoparticles is still unclear, motivating us to explore the molecular mechanism of N-XBSD formation. We studied the self-assembly of high abundant compounds in N-XBSD. Interestingly, we found that mulberroside A and kukoaMine B were able to form nanoparticles (MUL-KUB NPS), and liquiritin and kukoaMine B were also able to form nanoparticles (LOQ-KUB NPS). The self-assembly between them by electrostatic complexation was revealed by FT-IR and HRMS. This suggests that the mechanism of N-XBSD formation may be due to self-assembly between the compounds. The study not only provides an idea for revealing the formation mechanism of nanoparticles in TCM decoctions but also supplies a reference for discovering carrier-free nanoscale from TCM decoctions. The japonica rice in the prescription contains a large amount of proteins and polysaccharides, and in a study on the solubilizing effect of vinegar-roasted chai hu polysaccharides on insoluble drugs in traditional Chinese medicine, the polysaccharides self-assembled into micelles that encapsulated water-insoluble compounds through the interplay of hydrogen bonding and hydrophobic forces, which improved the bioavailability of baicalein and safranin.[30] There are also studies that have found that starch can form self-assembled nano systems with lipophilic drugs;[31] and the size of starch granules could be reduced to nanometer size by ball milling method.[32] We speculate that Japonica rice may act as a drug carrier in the prescription and can encapsulate most of the active compounds to form nanoparticles during the boiling process.

In the UPLC-MS/MS method for testing XBSD in rats, due to the low blood concentrations of kukoamine A, isoiquiritin apioside and mulberloside C, these three compounds were not selected for pharmacokinetic studies. KukoaMine B determination was interfered with by endogenous substances in plasma.[33] By adjusting the gradient elution conditions, we shifted the peak time of kukoaMine B backward, and separated the endogenous substances from kukoaMine B in the column as much as possible in order to reduce the matrix effect. The use of appropriate sample pretreatment methods is very important to reduce the matrix effects of endogenous components in plasma. Protein precipitation with organic reagents has higher recovery than liquid–liquid extraction and is simpler to operate than solid-phase extraction.[34] Therefore, the effects of methanol, acetonitrile, and methanol-acetonitrile (1:1, v/v) were compared for protein precipitation. The results showed that methanol precipitation of proteins was more effective in extracting the five analytes with lower endogenous interference. In addition, oral administration of liquiritin and liquiritin apioside to rats results in rapid absorption and elimination,[34,35] which is consistent with the results of the present study.

Pharmacokinetic study in rat showed that the bioavailability of mulberroside A, kukoaMine B, ligiritin, liquiritin apioside and glycyrrhizic acid ammonium salt were significantly higher after N-XBSD administration compared to the free drugs at the same administration concentration. In general, nanoparticles with sizes smaller than 500 nm and neutral or negatively charged surfaces promote mucus permeation, which is closely related to intestinal absorption. Therefore, the negatively charged N-XBSD has good intestinal permeation properties. The mechanisms of nanoparticles taken up by intestinal cells mainly include phagocytosis, caveolae-mediated endocytosis and macropinocytosis. Studies have shown that caveolae mediate endocytosis of 100 nm of nanoparticles and that caveolae-mediated endocytosis bypasses lysosomal degradation,[33] which suggests that NPs can enter the circulation in the form of nanoparticles after being absorbed by intestinal epithelial cells. In addition, intestinal epithelial cells have many efflux transporters, such as P-gp, that significantly reduce the uptake of their substrates. A study showed that natural nanoparticles in *Coptidis Rhizoma* extract were able to carry berberine, promote its uptake by Caco-2 cells through an indomethacin-sensitive endocytic mechanism, and reduce its efflux by the efflux transporter P-gp from intestinal epithelial cells.[5] Mulberroside A, liquiritin and glycyrrhizic acid ammonium salt in XBSD are all substrates of P-gp,[36–39] suggesting that nanoparticles may promote the intestinal absorption of mulberroside A, liquiritin and glycyrrhizic acid ammonium salt by inhibiting P-gp.

Nanoparticles in decoctions have received increasing attention in recent years. However, the current research mainly focuses on the nanoparticles isolation and their biological activities. In this study, we found that N-XBSD contains a large number of active ingredients and tried to explore the formation mechanism of N-XBSD. In addition, the pharmacokinetic differences between N-XBSD and free drug were compared for the first time. Considering the widespread presence of nanoparticles in herbal decoctions, we believe that the present study will stimulate more research on nanoparticles in decoctions to develop a more comprehensive understanding of their medicinal value.

Conclusions

In this study, the phases of XBSD were separated by dialysis combined with centrifugation, and three phases, S-XBSD, T-XBSD and N-XBSD, were obtained, and the morphology and particle size distribution of N-XBSD were characterized by using transmission electron microscopy and Malvern particle size apparatus. The contents of each phase were determined by HPLC, and most of the main active compounds in XBSD could be found in N-XBSD. And the formation mechanism of N-XBSD was revealed from the perspective of bimolecular self-assembly. An UPLC-MS/MS method was established for the determination of the levels of mulberroside A, kukoaMine B, ligiritin, liquiritin apioside and glycyrrhizic acid ammonium salt in the plasma of rats after administration of XBSD, which was successfully used for the comparison of the difference in the absorption of XBSD, N-XBSD, and free drugs. The results suggest that N-XBSD had similar pharmacokinetic behavior to XBSD. However, N-XBSD significantly increased the bioavailability of five active compounds compared to the free drugs. In conclusion, our methodology and findings may inspire further studies on the interaction of active phytochemicals with nanoparticles and their pharmacokinetics in TCM decoctions.

Abbreviations

AUC_{0-t}, area under curve from time zero to time t; $AUC_{0-\infty}$, area under curve from time zero to time infinity; C_{max}, maximum plasma concentration; CLz/F, clearance corrected for bioavailability; FT-IR, Fourier transform infrared spectroscopy; HPLC, high-performance liquid chromatography; HRMS, high-resolution mass spectrometry; IS, internal standard; LOQ, limit of quantification; MRT_{0-t}, mean residence time from time zero to time t; SCF, simulated colonic fluid; SGF, simulated gastric fluid; SIF, simulated intestinal fluid; TCM, traditional Chinese medicine; $T_{1/2}$, terminal elimination half-life; T_{max}, time to reach C_{max}; TEM, transmission electron microscopy; UPLC-MS/MS, ultra-performance liquid chromatography-tandem mass spectrometry.

Data Sharing Statement

The data supporting the findings of this study are available from the corresponding author upon reasonable request.

Ethics Approval and Informed Consent

All animal experimental protocols were approved by the Institutional Animal Care and Use Committee of Shanghai University of Traditional Chinese Medicine (PZSHUTCM220725022). All experiments were performed in accordance with the Guidelines for Care and Use of Laboratory Animals of Shanghai University of Traditional Chinese Medicine.

Disclosure

The authors report no conflicts of interest in this work.

References

1. Sun W, Shahrajabian MH. Therapeutic potential of phenolic compounds in medicinal plants-natural health products for human health. *Molecules*. 2023;28(4):1845.
2. Sun W, Shahrajabian MH, Cheng Q. Natural dietary and medicinal plants with anti-obesity therapeutics activities for treatment and prevention of obesity during lock down and in post-COVID-19 Era. *Appl Sci*. 2021;11(17):7889. doi:10.3390/app11177889
3. Shahrajabian MH, Sun W, Soleymani A, Cheng Q. Traditional herbal medicines to overcome stress, anxiety and improve mental health in outbreaks of human coronaviruses. *Phytother Res*. 2021;35(3):1237–1247. doi:10.1002/ptr.6888
4. Zhao Q, Luan X, Zheng M, et al. Synergistic mechanisms of constituents in herbal extracts during intestinal absorption: focus on natural occurring nanoparticles. *Pharmaceutics*. 2020;12(2):128. doi:10.3390/pharmaceutics12020128
5. Zhao J, Zhao Q, Lu JZ, et al. Natural nano-drug delivery system in coptidis rhizoma extract with modified berberine hydrochloride pharmacokinetics. *Int J Nanomed*. 2021;16:6297–6311. doi:10.2147/IJN.S323685
6. Wang CH, Cheng XM, Bligh SWA, et al. Pharmacokinetics and bioavailability of gentiopicroside from decoctions of Gentianae and Longdan Xiegan Tang after oral administration in rats—Comparison with gentiopicroside alone. *J Pharm Biomed Anal*. 2007;44(5):1113–1117. doi:10.1016/j.jpba.2007.04.036
7. Zhuang Y, Yan J, Zhu W, et al. Can the aggregation be a new approach for understanding the mechanism of Traditional Chinese Medicine? *J Ethnopharmacol*. 2008;117(2):378–384. doi:10.1016/j.jep.2008.02.017
8. Lü S, Su H, Sun S, et al. Isolation and characterization of nanometre aggregates from a Bai-Hu-Tang decoction and their antipyretic effect. *Sci Rep*. 2018;8(1):12209. doi:10.1038/s41598-018-30690-5
9. Ping Y, Li Y, Lü S, et al. A study of nanometre aggregates formation mechanism and antipyretic effect in Bai-Hu-Tang, an ancient Chinese herbal decoction. *Biomed Pharmacother*. 2020;124:109826. doi:10.1016/j.biopha.2020.109826
10. Lin D, Du Q, Wang H, et al. Antidiabetic micro-/nanoaggregates from ge-gen-qin-lian-tang decoction increase absorption of baicalin and cellular antioxidant activity in vitro. *Biomed Res Int*. 2017;2017:9217912. doi:10.1155/2017/9217912
11. Zhang Q, Gao Y, Wang Y, et al. Particle size of "Cuo San" of famous classical formulas and decoction process with Xiebai San for example. *Zhongguo Zhong Yao Za Zhi*. 2020;45(4):878–883. doi:10.19540/j.cnki.cjcmm.20191001.305
12. Piao SJ, Chen LX, Kang N, et al. Simultaneous determination of five characteristic stilbene glycosides in root bark of Morus albus L. (Cortex Mori) using high-performance liquid chromatography. *Phytochem Anal*. 2011;22(3):230–235. doi:10.1002/pca.1270
13. Hsu JH, Yang CS, Chen JJ. Antioxidant, Anti-α-glucosidase, antityrosinase, and anti-inflammatory activities of bioactive components from Morus alba. *Antioxidants*. 2022;11(11):2222. doi:10.3390/antiox11112222
14. Chen H, Olatunji OJ, Zhou Y. Anti-oxidative, anti-secretory and anti-inflammatory activities of the extract from the root bark of Lycium chinense (Cortex Lycii) against gastric ulcer in mice. *J Nat Med*. 2016;70(3):610–619. doi:10.1007/s11418-016-0984-2
15. Gao D, Li Q, Liu Z, et al. Hypoglycemic effects and mechanisms of action of *cortex lycii radicis* on alloxan-induced diabetic mice. *Yakugaku Zasshi*. 2007;127(10):1715–1721. doi:10.1248/yakushi.127.1715
16. Chen JZ, Lu X, Hu Y-Q, et al. Research progress on chemical constituents and pharmacological studies on root bark of Lycium barbarum. *Zhongguo Zhong Yao Za Zhi*. 2021;46(12):3066–3075. doi:10.19540/j.cnki.cjcmm.20210223.601
17. Lyu W, Qin W, Zhang J, et al. Inhibitory effects of Kukoamine B on the inflammatory response of small intestine in lipopolysaccharide-induced septic mice and its potential mechanisms. *Zhonghua Wei Zhong Bing Ji Jiu Yi Xue*. 2015;27(2):121–126. doi:10.3760/cma.j.issn.2095-4352.2015.02.009

18. Bian M, Zhen D, Shen Q-K, et al. Structurally modified glycyrrhetinic acid derivatives as anti-inflammatory agents. *Bioorg Chem*. 2021;107:104598. doi:10.1016/j.bioorg.2020.104598

19. Cheng Y, Zhong X, Nie X, et al. Glycyrrhetinic acid suppresses breast cancer metastasis by inhibiting M2-like macrophage polarization via activating JNK1/2 signaling. *Phytomedicine*. 2023;114:154757. doi:10.1016/j.phymed.2023.154757

20. Zhou H, Yang T, Lu Z, et al. Liquiritin exhibits anti-acute lung injury activities through suppressing the JNK/Nur77/c-Jun pathway. *ChinMed*. 2023;18(1):35. doi:10.1186/s13020-023-00739-3

21. Kuang Y, Li B, Fan J, et al. Antitussive and expectorant activities of licorice and its major compounds. *Bioorg Med Chem*. 2018;26(1):278–284. doi:10.1016/j.bmc.2017.11.046

22. Song J, Kim JY, You G, et al. Formulation of glycyrrhizic acid-based nanocomplexes for enhanced anti-cancer and anti-inflammatory effects of curcumin. *Biotechnol Bioprocess Eng*. 2022;27(2):163–170. doi:10.1007/s12257-021-0198-7

23. Ma BL, Yin C, Zhang B-K, et al. Naturally occurring proteinaceous nanoparticles in Coptidis Rhizoma extract act as concentration-dependent carriers that facilitate berberine absorption. *Sci Rep*. 2016;6:20110. doi:10.1038/srep20110

24. Zhang M, Xiao B, Wang H, et al. Edible ginger-derived nano-lipids loaded with doxorubicin as a novel drug-delivery approach for colon cancer therapy. *Mol Ther*. 2016;24(10):1783–1796. doi:10.1038/mt.2016.159

25. Ke LJ, Gao G-Z, Shen Y, et al. Encapsulation of aconitine in self-assembled licorice protein nanoparticles reduces the toxicity in vivo. *Nanoscale Res Lett*. 2015;10(1):449. doi:10.1186/s11671-015-1155-1

26. Liu Y. Optimization of preparation technology of standard decoction of Xiebaisan based on fingerprint and quality value transmitting. *Lishizh Med Materia Medica Res*. 2022;33(01):125–129.

27. Zhao G, Hong L, Liu M, et al. Isolation and characterization of natural nanoparticles in naoluo xintong decoction and their brain protection research. *Molecules*. 2022;27:5.

28. Zhou J, Gao G, Chu Q, et al. Chromatographic isolation of nanoparticles from Ma-Xing-Shi-Gan-Tang decoction and their characterization. *J Ethnopharmacol*. 2014;151(3):1116–1123. doi:10.1016/j.jep.2013.12.029

29. Wu H, Nan J, Yang L, et al. Insulin-loaded liposomes packaged in alginate hydrogels promote the oral bioavailability of insulin. *J Control Release*. 2023;353:51–62. doi:10.1016/j.jconrel.2022.11.032

30. Zhao Y, Wan P, Wang J, et al. Polysaccharide from vinegar baked radix bupleuri as efficient solubilizer for water-insoluble drugs of Chinese medicine. *Carbohydr Polym*. 2020;229:115473. doi:10.1016/j.carbpol.2019.115473

31. Zhang Z, Huang J, Jiang S, et al. Porous starch based self-assembled nano-delivery system improves the oral absorption of lipophilic drug. *Int J Pharm*. 2013;444(1–2):162–168. doi:10.1016/j.ijpharm.2013.01.021

32. Jhan F, Gani A, Noor N, et al. Characterisation and utilisation of nano-reduced starch from underutilised cereals for delivery of folic acid through human GI tract. *Sci Rep*. 2021;11(1):4873. doi:10.1038/s41598-021-81623-8

33. Wang Z, Zhao Q, Li L, et al. Development and validation of a rapid and sensitive UPLC–MS/MS method for quantification of kukoamine B in human plasma: application to a clinical pharmacokinetic study. *J Pharm Biomed Anal*. 2017;132:1–6. doi:10.1016/j.jpba.2016.09.032

34. Huang P, Tang Y, Li C, et al. Correlation study between the pharmacokinetics of seven main active ingredients of Mahuang decoction and its pharmacodynamics in asthmatic rats. *J Pharm Biomed Anal*. 2020;183:113144. doi:10.1016/j.jpba.2020.113144

35. Lu YY, Chen JF, Song JY, et al. Pharmacokinetics study of 16 representative components from Baoyuan Decoction in rat plasma by LC–MS/MS with a large-volume direct injection method. *Phytomedicine*. 2019;57:148–157. doi:10.1016/j.phymed.2018.09.002

36. Chen LC, Cheng WJ, Lin SY, et al. CPT11 with P-glycoprotein/CYP 3A4 dual-function inhibitor by self-nanoemulsifying nanoemulsion combined with gastroretentive technology to enhance the oral bioavailability and therapeutic efficacy against pancreatic adenocarcinomas. *Drug Deliv*. 2021;28(1):2205–2217. doi:10.1080/10717544.2021.1989087

37. He Y, Ci X, Xie Y, et al. Potential detoxification effect of active ingredients in liquorice by upregulating efflux transporter. *Phytomedicine*. 2019;56:175–182. doi:10.1016/j.phymed.2018.10.033

38. Li YH. Reversal effect of mulberroside A on the multidrug resistance in K562/Adriamycin-resistant cell. *The Chinese J Clin Pharmacol*. 2022;38 (10):1064–1068.

39. Ma ZX. lmpact of " Zao-ji-sui-yuan" Combined with glycyrrhizae on rat lntestinal p-glycoprotein transport function in vitro. *J Nanjing Univ Traditional Chin Med*. 2016;32(04):352–355.

40. Sahay G, Alakhova DY, Kabanov AV. Endocytosis of nanomedicines. *J Control Release*. 2010;145(3):182–195. doi:10.1016/j.jconrel.2010.01.036